Simulation of Progressive Damage in Bolted Composite Joints

Hannes Koerber, Pedro P. Camanho

DEMEGI, Faculdade de Engenharia, Universidade do Porto
Rua Dr. Roberto Frias, 4200-465 Porto, Portugal
hkoerber@fe.up.pt

Abstract

In this article, finite element analyses of mechanically fastened double-lap joints in carbon/epoxy laminates are performed using a progressive damage model available in the commercial software ABAQUS. An alternative damage model, implemented into a VUMAT user subroutine, is also presented. Two failure modes are considered: catastrophic net-section tension-failure and non-catastrophic accumulation of bearing damage. A three-dimensional mesh is used for the analysis and in addition to results for static implicit analysis; a method for explicit simulation of quasi-static tests is presented. The simulation results are compared with experimental data. By comparison of the two damage models for the tension-failure simulation, it can be shown that the shape of the damage evolution law for fiber-tension damage is perhaps more critical than the fracture energy value. Results for simulation of bearing damage using the commercial damage model are presented and some limitations of the model are discussed.

1 Introduction

With the increasing use of fiber-reinforced plastics (FRPs) in aerospace structures, the analysis of mechanically fastened joints in composite materials has become a key aspect in the design process. It is well known that mechanically fastened joints perform better in metals than they do in composite structures. The joint efficiency in a metal structure is 70% - 80% compared to 40% - 50% in a composite [1]. Some reasons for the relatively low performance of bolted composite joints are: the brittleness of the composite material, which allows little stress relief around the loaded hole; material anisotropy, leading to high stress concentrations; and low through-thickness strength of classic unidirectional laminates, causing interlaminar delamination. Despite these disadvantages, mechanically fastened composite joints are widely used, since they provide a fast and efficient way of substructure assembly. Due to the complex failure mechanisms, their design however relies heavily on experiments combined with semi-analytical methods [2]. If it is possible to obtain part of the mechanical properties needed during the design phase via numerical analysis, significant cost savings can be achieved. Analysis using progressive damage models, able to capture the physics of the failure mechanisms occurring at damage initiation and damage evolution leading to ultimate failure has therefore received significant attention in recent years.

In general, two-dimensional finite element modelling is sufficient for the majority of linear composite laminate analysis. While this is computational efficient and preferable for most applications, a three-dimensional model may be suited better for the analysis of a bolted composite joint in a quasi-isotropic laminate. In a 3D-model, cohesive zone elements can be included to capture delamination failure; unsymmetrical loading of the bolt hole (single-lap joints) can be considered and through-thickness stresses (clamping forces) which are known to have a significant effect on the initiation of bearing damage may be considered [3].

2 Progressive Damage Models for Unidirectional FRP Laminates

Two progressive damage models for FRP unidirectional laminates are applied in the present work. The first model recently became available in the commercial finite element code ABAQUS/Standard 6.6.1 and ABAQUS/Explicit 6.7.1, and will therefore be referred to as the Abaqus-Model. The Hashin-criteria is used for damage initiation in this model [4],[5]. The influence of damage on the constitutive material model is based on the work of Matzenmiller et al. [6] and damage evolution for all failure modes is governed by a simple linear formulation, used by Camanho and Davila for cohesive elements [7]. A detailed description of the Abaqus-Model, including its numerical implementation, is presented in [8]. An alternative damage model, based on the work of Maimi et al. [9] is also used in this study. The model can be used for finite element analysis in Abaqus/Explicit via a VUMAT user subroutine and will therefore be referred to as the VUMAT-Model. Maimi applies a combination of the LaRC03 and LaRC04 criteria for damage initiation [10],[11]. Rather than using linear softening, exponential damage evolution laws are applied to describe the softening response for all failure modes except fiber tension. For unidirectional carbon/epoxy laminates, such as the material used in this study, the propagation of a crack perpendicular to the fiber-direction under tensile loading can be divided into two phases. An initial and rather brittle fiber-matrix failure mechanism, followed by a tougher fiber-bridging and fiber pull-out phase acting at a lower stress level [12]. To account for the different damage mechanisms, a linear-exponential law is therefore used for the fiber-tension mode (Figure 1, b). For both models, the area under the stress-strain curve is equal to the dissipated fracture energy divided by a characteristic length of the finite element. References [8] and [9] provide further information on the determination of the characteristic element length. In case of the VUMAT-Model, the fracture toughness determined for fiber-tensile fracture (Table 2) is divided in two parts, associated with the linear and exponential softening law. In addition to the tensile strength X^T, a value representing the fiber pull-out strength X^{PO} must be specified for the VUMAT-model.

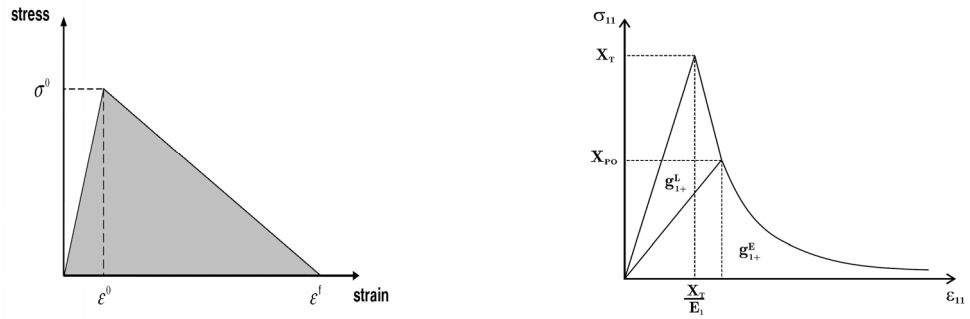

(a) Abaqus-model [8] (b) VUMAT-model [9]

Figure 1. Damage evolution laws for fiber-tension

3 Experiments

Two double-shear bolted joint specimens tested in the context of developing a design methodology for mechanically fastened composite joints [2] were selected in this study. The specimen geometry and dimensions are shown in Figure 2 and were designed to either promote pure tensile- or bearing-failure. Both specimens were made of UD carbon/epoxy prepreg Hexcel IM7-8552 with a quasi-isotropic lay-up of

$[90/0/+45/-45]_{4s}$. A 6 mm steel bolt was used and a washer with an outer-diameter of 12 mm was placed on either side of the laminate. The torque applied to the bolt corresponds to a finger-tight assembly. Surface strain was measured according to the strain gauge positions specified in Figure 2. Both specimens were tested in a conventional load frame at a quasi-static displacement-rate of 2 mm/min.

Failure Mode	t	l	w	d	e	l_1	l_2
Bearing	3	215	36	6	18	9	50
Tension	3	200	12	6	24	15	50

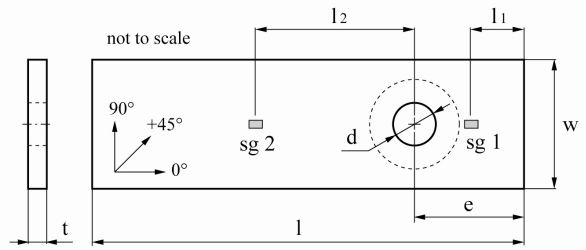

Figure 2. Specimen geometry (dimensions in mm)

4 FE Model

The finite element model used for both specimen types will be explained on the basis of the tension failure specimen shown in Figure 3. For the bearing failure specimen a similar mesh was used. Due to the lay-up symmetry, only half of the laminate was modelled and symmetry boundary conditions were applied at the laminate symmetry plane. One element per ply was used for the laminate mesh, which was divided into a coarse mesh area away from the hole and a refined mesh area around the hole and in the direction of loading. Both mesh regions are connected via a TIE constraint which is a convenient way for mesh transition as opposed to a paved mesh or multi-point constraint (MPC). In case of the bolt, only the length of the shaft in contact with the hole was modelled. Similar symmetry boundary conditions were applied to the nodes lying in the laminate symmetry plane. The washer is accounted for by a distributed load corresponding to the bolt torque and applied to a surface approximately equal to the surface area of the washer. Strain in the loading direction is obtained from two element sets in the first layer of elements, representing the 90° outer-ply, at the strain gauge position of the test specimen (Figure 2). Although not applied in the present simulations, the 3D finite element mesh was developed for the use of cohesive zone delamination elements and a full 3D-formulation of the VUMAT damage model, which is yet to be implemented into an Abaqus subroutine. For the Abaqus-Model, where two formulations of the Hashin-criteria are available, the formulation proposed by Hashin and Rotem was selected [4]. The in-situ effect was considered for both damage models. It is characterised by higher transverse tensile and shear strengths for a ply constrained by plies with different fiber orientations, compared to the strengths of the same ply in a unidirectional laminate [13]. For the tension-failure specimen, simulations were conducted using the implicit and explicit Abaqus-model as well as the VUMAT-model. The bearing failure specimen was simulated using the implicit and explicit Abaqus-model. Depending on the damage model and solver, different elements were used for the different regions of the finite element model. The selected elements are summarised in Table 1 where SC8R stands for a reduced integration continuum shell element, similar to a standard solid but with a kinematic and a constitutive behaviour similar to a conventional shell. The Abaqus-Model is limited to elements with plane-stress formulation, therefore only the SC8R element can be used in a 3D-mesh. C3D8 and C3D8R represent standard solid elements in a fully integrated or reduced integration

formulation, respectively. For reduced integration elements, default hourglass control parameters were selected. In case of the implicit Abaqus-model, viscous regularisation (VR) had to be used to obtain a converging solution. The VR-parameters were selected according to a similar example given in [8].

Table 1. Finite element selection

Solver		Damage	Mesh Area		
Type	Version	Model	Laminate Fine	Laminate Coarse	Bolt
Abaqus/Standard	6.6.1	Abaqus	SC8R	C3D8	C3D8
Abaqus/Explicit	6.7.1	Abaqus	SC8R	C3D8R	C3D8R
Abaqus/Explicit	6.6.1	VUMAT	C3D8R	C3D8R	C3D8R

The joint is loaded via a velocity boundary condition applied to a selected node-set of the bolt mesh. In case of the implicit Abaqus-model, this velocity corresponds to the actual test speed. To obtain a simulation time suited for an explicit simulation, two modifications were applied to the explicit model. The test speed was increased by a factor of 1000 and the mass density was scaled by a factor of 100, resulting in a 10-fold increase of the stable time increment.

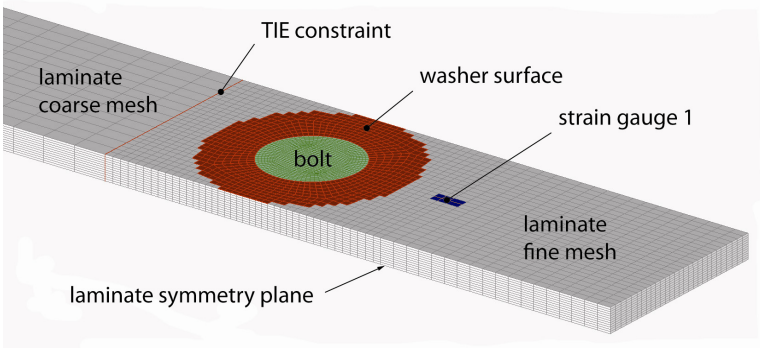

Figure 3. Finite element model of tension failure specimen

To evaluate if the modified FE-model produces an appropriate quasi-static response, the energy balance was studied [14]:

$$E_I + E_V + E_{FD} + E_{KE} - E_W = E_{TOTAL} = const. \tag{4.1}$$

E_I is the internal energy, E_V is the energy absorbed by viscous dissipation, E_{FD} is the energy absorbed by frictional dissipation, E_{KE} is the kinetic energy, E_W is the work of external forces and E_{TOTAL} is the total energy in the system. For a quasi-static analysis, E_W should be approximately equal to E_I, while as E_V, E_{FD}, E_{KE} and E_{TOTAL} should be near zero. According to [14] however, a 5% to 10% value of the kinetic energy compared to the internal energy is acceptable. A graphical representation of the energy-balance is illustrated in Figure 4. With the exception of a slight increase in the total energy E_{TOTAL}, the above conditions for a quasi-static analysis hold for the entire duration of the simulation. The total energy increase prior to ultimate failure is caused by an increase of E_V and E_A. These two energies are introduced to stabilise the

element during damage evolution. As they remain small compared to E_I and E_W, it was concluded that the modifications to the explicit model are valid and the simulation is in fact representing a quasi-static test.

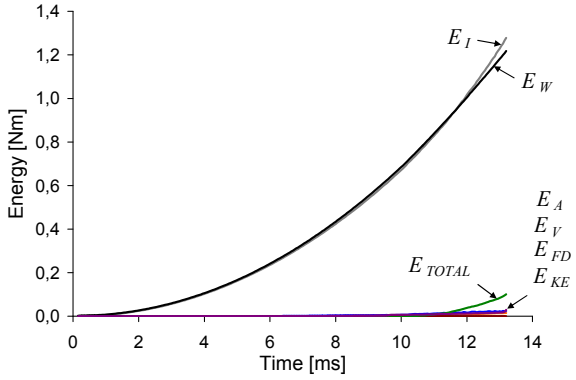

Figure 4. Energy balance, tension-failure simulation (VUMAT-model)

The material properties used for both progressive damage models are summarised in Table 2. Elastic and unidirectional ply strengths can be obtained from standard test methods and the in-situ ply strengths can be calculated according to [13]. For the fracture energies, a test standard exists only for matrix tension [15]. The values for tensile and compressive fiber fracture, can be obtained from compact tension (CT) and compact compression (CC) tests as proposed by Pinho et al. [16]. Matrix compression fracture energy can be obtained from mode II end-notched flexure tests (ENF) and a formulation for G_{2-} specified in [9]. According to this formulation, the value depends on the laminate stacking configuration. In the present study the value for a strongly confined laminate is used. The additional parameters used for the VUMAT-model are associated with the different damage evolution law (compare Figure 1, b) and since the LaRC damage initiation criteria considers the fracture angle for compressive transverse load cases, a representative fracture angle α must also be given.

Table 2. IM7-8552 material properties

(a) Elastic ply properties

E_1	171.42	GPa
$E_2 = E_3$	9.08	GPa
$G_{12} = G_{13}$	5.29	GPa
G_{23}	3.98	GPa
$\nu_{12} = \nu_{13}$	0.32	-
ν_{23}	0.5	-

(b) UD ply strength

X^T	2226.2	MPa
X^C	1200.1	MPa
Y^T_{ud}	62.3	MPa
Y^C	199.8	MPa
S^L_{ud}	92.3	MPa

(c) In-situ ply strength [MPa]

Ply configuration	Y^T_{is}	S^L_{is}
thin outer	101.4	107.0
thin embedded	160.2	130.2
thin embedded (2t)	113.3	107.0

(d) Fracture energies [kJ/m²]

fiber tension	G_{1+}	81.5
fiber compression	G_{1-}	106.5
matrix tension	G_{2+}	0.2774
matrix compression	G_{2-}	5.62

(e) Additional VUMAT-model properties

fiber pull-out strength	X_{PO}	232.3	MPa
fracture angle	α	53	°
G_{1+}, linear softening	G^L_{1+}	31.5	kJ/m²
G_{1+}, exponential softening	G^E_{1+}	50.0	kJ/m²

5 Simulation Results

5.1 Tension-failure simulation

The maximum load, P_{max}, obtained from the simulations and experiment, is summarised in Table 3 and Figure 5 shows the load-strain response at strain gauge position 1 and 2. It can be seen that both simulations using the Abaqus-model significantly overestimate the ultimate load while as the results of the VUMAT-model correlate well with the mean average load maximum obtained from the experiment. Another difference between the simulation results can be noticed when plotting the fiber damage parameter for a 0°-ply (Figure 6). For both Abaqus-model simulations, the crack propagates at an angle of about 45° to the fiber-direction and hence follows the matrix damage developing in the neighbouring 45°-ply. The crack in the VUMAT-model localises in a plane perpendicular to the fibers, as observed in the experiment.
It should be noted that various damping mechanisms, such as mass- or stiffness-proportional Rayleigh-damping and bulk viscosity, exist for the Abaqus-model while as these mechanisms did not have a major effect on the user material specified in the VUMAT subroutine. Therefore oscillations measured at strain gauge 1 could not be avoided in this case.

Table 3. Maximum load, tension failure specimen

		P_{max} [kN]	
Experiment	(mean average)	9.477	
	(minimum)	9.232	(-2.6%)
	(maximum)	10.135	(+6.9%)
Abaqus Model, implicit		12.833	(+35.4%)
Abaqus Model, explicit		13.122	(+38.5%)
VUMAT Model		9.454	(-0.2%)

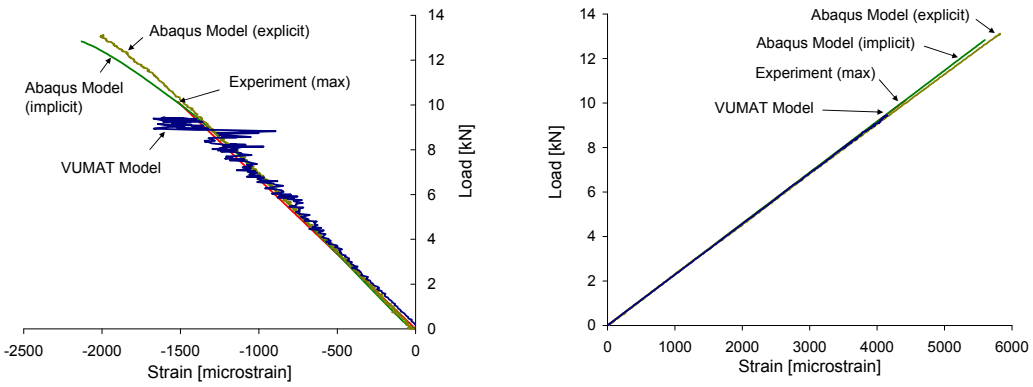

(a) Strain gauge 1 (b) Strain gauge 2

Figure 5. Load-strain response, tension-failure specimen

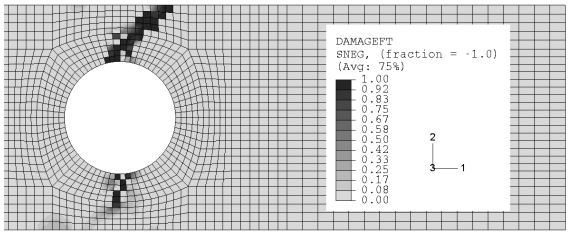

(a) Abaqus-model, implicit static

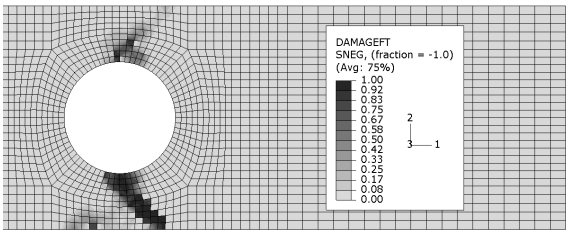

(b) Abaqus-model, explicit

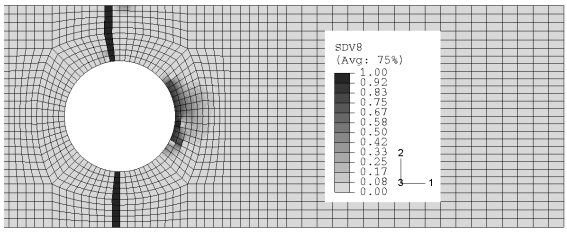

(c) VUMAT-model

Note: For the Abaqus-model, a separate damage parameter exists for fiber-tension and fiber-compression damage. In case of the VUMAT-model, fiber-tension and fiber-compression damage are combined in one parameter. Therefore, diagram (c) also shows fiber-compression damage at the bolt-hole contact interface.

Figure 6. Fiber damage in layer 2 (0°) at maximum load, tension failure specimen

5.2 Bearing-failure simulation

Other than in the case of the tension-failure specimen, where ultimate failure is clearly defined by the maximum load, bearing-failure is a non-catastrophic damage mode, characterised by a progressive accumulation of damage and permanent hole deformation [2]. As a result, different definitions may be used for defining bearing strength such as the onset of nonlinearity or the bearing strength at 2% bearing strain offset. Figure 7 (a) shows the load-strain response obtained from simulation and a representative experiment at strain gauge position 1. Diagram (b) illustrates the bearing stress-bearing strain curve as defined by the ASTM test method [17]. The difference between the initial bearing stress slope of simulation and experiment can be explained by the different method of obtaining the hole elongation. In case of the simulation, the elongation was measured directly on the hole, while as for the test a LVDT was attached to the test rig and laminate, similar to the illustration in Fig. 10 (a) of [17].

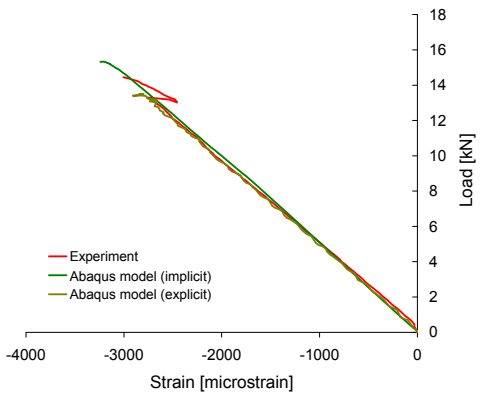

(a) Load-strain response at strain gauge 1

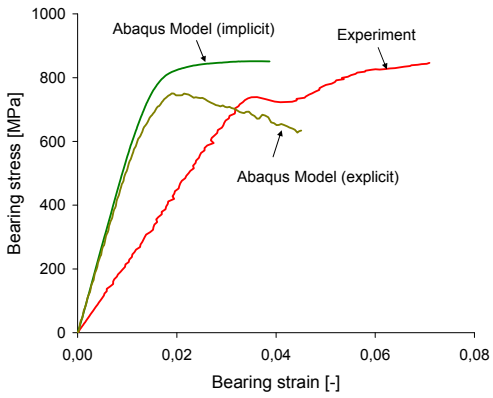

(b) Bearing stress – bearing strain

Figure 7. Load-strain and bearing stress-bearing strain response

Table 4 summarises the bearing strengths defined at the onset of nonlinearity σ_{onl}^{br} and at 2% bearing strain offset $\sigma_{2\%off}^{br}$ for the implicit and explicit Abaqus-model simulation and the experiment. It is clear from the experimental results that the 2% offset definition is associated with significant data scatter which complicates a comparison between simulation and experiment. It was shown by Camanho and Lambert that damage at 2% strain offset has progressed to a state of through-the-thickness cracks spanning several plies [2]. This damage state can not be captured by the present finite element model and therefore the onset of nonlinearity (at 5% decrease of the initial chord modulus), is used for a comparison of simulation and experiment rather than the 2% offset definition. For both simulations, the predicted bearing strength is below the experimental value. Figure 8 shows the extent of predicted fiber-compression damage at 2% offset bearing strength.

Table 4. Bearing strength

		σ_{onl}^{br} [MPa]		$\sigma_{2\%off}^{br}$ [MPa]	
Experiment	(mean average)	747		870	
	(minimum)	738	(-1.2%)	747	(-14.1%)
	(maximum)	753	(+0.8%)	958	(+10.1%)
Abaqus-model, implicit		645	(-13.6%)	851	(-2.2%)
Abaqus-model, explicit		610	(-18.3%)	689	(-20.8%)

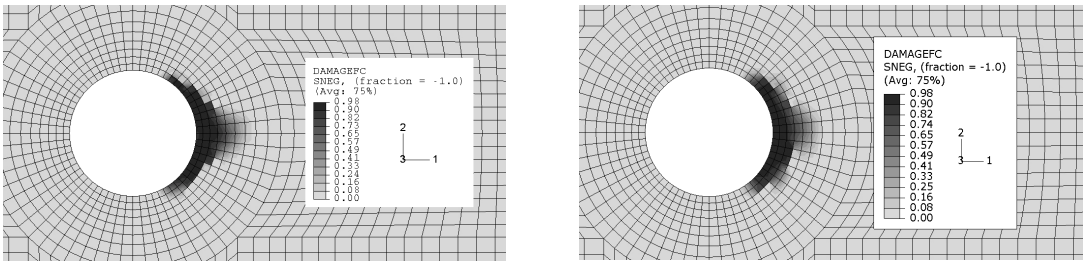

(a) Abaqus-model, implicit static (b) Abaqus-model, explicit

Figure 8. Fiber damage in layer 2 (0°) at 2% offset bearing strength, bearing specimen

6 Discussion and Conclusion

6.1 Tension-failure simulation

In Section 5.1 it was shown that the ultimate load for the tension-failure specimen was significantly over-predicted by the Abaqus-model (Table 3). Since the same material properties were used for all simulations and viscous regularisation was not specified for the explicit analysis, it is assumed that the difference between the Abaqus- and VUMAT-model is associated with the damage evolution law. It was further noticed that the crack for the Abaqus-model develops in a plane inclined at an angle of 45° to the fibers. In an attempt to create a damage evolution shape similar to that used in the VUMAT-model, the fracture energy for fiber-tension (compare Table 2, d) was reduced by 50%. With this modification, the over-prediction was reduced to 7.8% for the implicit and to 18.5% for the explicit formulation of the Abaqus-model. Comparing Figure 6 and Figure 8, it can be seen that the crack has shifted towards a plane

perpendicular to the fiber-direction with the improvement most pronounced for the implicit model. It is therefore concluded that the shape of the fiber-tension damage evolution law is more critical than the actual fracture toughness value and that the formulation chosen in the VUMAT-model is able to represent the damage mechanisms occurring in the fiber-tension damage mode.

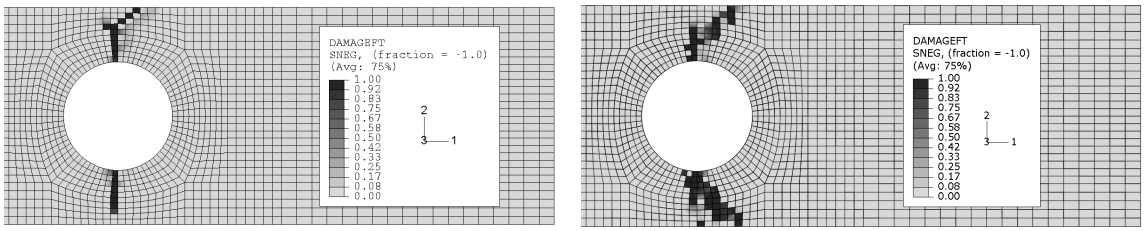

(a) Abaqus-model, implicit static (b) Abaqus-model, explicit

Figure 9. Fiber-damage in layer 2 (0°) at maximum load for Abaqus-model with modified fracture toughness

6.2 Bearing-failure simulation

In Section 5.2 it was shown that conservative results can be obtained for the bearing strength at onset of nonlinearity (ONL), using either the implicit or explicit formulation of the Abaqus-model (Table 4). With damage initiation occurring at a similar stress level of about 450-460 MPa, the bearing strength results for the ONL-formulation of bearing strength were relatively close. The difference in the nonlinear region of the bearing stress curve, comparing the implicit and explicit solution in Figure 7 is not entirely understood yet and may partly be attributed to the influence of viscous regularisation on the evolution of damage. As for the tension-failure specimen, viscous regularisation had to be used for the implicit static simulation in order to obtain a converging solution but was not used in case of the explicit simulations. Further, it is possible that the masses considered in the explicit simulation, and hence the modifications as described in Section 4, may have an influence on the fiber-compression damage mode; although this did not seem to be critical for the tension-failure simulation.

It is concluded that the Abaqus-model, using a simple maximum strength criteria and linear damage evolution law for fiber-compression, is able to predict a lower bound for ONL bearing strength. In reality however, the damage mechanism for fiber-compression is more complicated with fiber-kinking occurring in the 0° plies. Further, the model can not account for the stabilising-effect of through-thickness stresses [3], which is not critical if a relatively low level of clamping pressure is used, but may lead to a significant under-prediction at higher torque-levels.

Acknowledgements

The financial support by the Air Force Office of Scientific Research, Air Force Material Command, USAF, under grant number FA8655-06-1-3072 is acknowledged. The U.S. Government is authorised to reproduce and distribute reprints for Governmental purpose notwithstanding any copyright notation thereon.

References

[1] McCarthy M.A., "BOJCAS: Bolted Joints in Composite Aircraft Structures", *Air and Space Europe*, 2001; 3

[2] Camanho P.P., Lambert M., "A design methodology for mechanically fastened joints in laminated composite materials", *Composites Science and Technology*, 2006; 66: 3004-3020

[3] Park H.J, "Effects of stacking sequence and clamping force on the bearing strength of mechanically fastened joints in composite laminates", *Composite Structures*, 2001; 53: 213-221

[4] Hashin Z., Rotem A., "A fatigue failure criterion for fiber reinforced materials", *Journal of Composite Materials*, 1973; 7: 448-464

[5] Hashin Z., "Failure criteria for unidirectional fiber composites", *Journal of Applied Mechanics*, 1980; 47: 329-334

[6] Matzenmiller A., Lubliner J., Taylor R.L., „A constitutive model for anisotropic damage in fiber-composites", *Mechanics of Materials*, 1995; 20: 125-152

[7] Camanho P.P., Davila C.G., "Mixed-mode decohesion finite elements for the simulation of delamination in composite materials", *NASA-TM-2002-211737*, 2002

[8] Lapczyk I., Hurtado J.A., "Progressive damage modelling in fiber-reinforced materials", *Composites Part A*, 2007; 38: 2333-2341

[9] Maimi P., Camanho P.P., Mayugo J.A., Davila C.G., "A continuum damage model for composite laminates: Part II – Computational implementation and validation", *Mechanics of Materials*, 2007; 39: 909-919

[10] Davila C.G., Camanho P.P., Rose C.A., "Failure criteria for FRP laminates", *Journal of Composites Materials*, 2005; 29: 323-345

[11] Pinho S.T., Davila C.G., Iannucci L., Robinson P., "Failure models and criteria for FRP under in-plane or three-dimensional stress states including shear non-linearity", *NASA-TM-2005-213530*, 2005

[12] Davila C.G., Rose C.A., "Superposition of cohesive elements to account for R-curve toughening in the fracture of composites", *Abaqus Users' Conference*, 2008

[13] Camanho P.P., Davila C.G., Pinho S.T., Iannucci L., Robinson P., "Prediction of in situ strengths and matrix cracking in composites under transverse tension and in-plane shear", *Composites Part A*, 2006; 37: 165-176

[14] ABAQUS 6.6 "Getting started with ABAQUS", Abaqus Inc., 2006

[15] "Standard test method for mode I interlaminar fracture toughness of unidirectional fiber-reinforced polymer matrix composites" ASTM D 5528-01, American Society for Testing and Materials (ASTM), West Conshohocken, PA, USA

[16] Pinho S.T., Robinson P., Iannucci L., "Fracture toughness of the tensile and compressive fibre failure modes in laminated composites", *Composites Science and Technology*, 2006; 66: 2069-2079

[17] "Standard test method for bearing response of polymer matrix composite laminates" ASTM D 5961/D 5961 M-05, American Society for Testing and Materials (ASTM), West Conshohocken, PA, USA